CHAPTER 7

RADIATIVE EXCHANGE BETWEEN NONIDEAL SURFACES

7.1 INTRODUCTION

In Chapter 6 we saw that, in certain situations, the directional nature of the reflectance of surfaces can strongly influence radiative heat transfer rates. This effect occurs particularly in open configurations, in enclosures with long channels, or in applications with collimated irradiation. Since real surfaces are neither diffuse nor specular reflectors, the actual directional behavior may have substantial impact, as we saw from the data in Fig. 6-17. We also noted that solar collectors did not appear to perform very well because, in our gray analysis, the reradiation losses were rather large. However, experience has shown that reradiation losses can be reduced substantially if *selective surfaces* (i.e., strongly nongray surfaces) are used for the collector plates. Apparently, there are a substantial number of applications for which our idealized treatment (gray, diffuse—i.e., direction-independent—absorptance and emittance, gray and diffuse or specular reflectance) is not sufficiently accurate. Actual surface properties deviate from our idealized treatment in a number of ways:

1. As seen from the discussion in Chapter 3, radiative properties can vary appreciably across the spectrum.
2. Spectral properties and, in particular, spectrally averaged properties may depend on the local surface temperature.
3. Absorptance and reflectance of a surface may depend on the direction of the *incoming* radiation.
4. Emittance and reflectance of a surface may depend on the direction of the *outgoing* radiation.
5. The components of polarization of incident radiation are reflected differently by a surface. Even for unpolarized radiation this difference can cause errors if many consecutive specular reflections take place. In the case of polarized laser irradiation this effect will always be important.

In this chapter we shall briefly discuss how nongray effects may be incorporated into the analyses of the previous chapters. We shall also develop the governing equation for the intensity leaving the surface of an enclosure with arbitrary radiative properties (spectrally and directionally), from which heat transfer rates may be calculated. This expression will be applied to a simple geometry to show how directionally irregular surface properties may be incorporated in the analysis.

7.2 RADIATIVE EXCHANGE BETWEEN NONGRAY SURFACES

In this section we shall consider radiative exchange between nongray surfaces that are directionally ideal: Their absorptances and emittances are independent of direction, while their reflectance is idealized to consist of purely diffuse and/or specular components. For such a situation equation (6.22) becomes, on a spectral basis,

$$\sum_{j=1}^{N} \left[\delta_{ij} - (1-\rho_{\lambda j}^{s})F_{\lambda,i-j}^{s}\right] E_{b\lambda j} = \sum_{j=1}^{N} \left(\frac{\delta_{ij}}{\epsilon_{\lambda j}} - \frac{\rho_{\lambda j}^{d}}{\epsilon_{\lambda j}} F_{\lambda,i-j}^{s}\right) q_{\lambda j} + H_{o\lambda i}^{s}, \qquad i = 1, 2, \ldots, N. \tag{7.1}$$

While diffuse view factors are purely geometric quantities and, therefore, never depend on wavelength, the specular view factors depend on the spectral variation of specular reflectances. In principle, equation (7.1) may be solved for all the unknown $q_{\lambda j}$ and/or $E_{b\lambda j}$. This operation is followed by integrating the results over the entire spectrum, leading to

$$q_j = \int_0^\infty q_{\lambda j}\, d\lambda, \qquad E_{bj} = \int_0^\infty E_{b\lambda j}\, d\lambda. \tag{7.2}$$

In matrix form this may be written, similar to equation (6.23), as

$$\mathbf{A}_\lambda \cdot \mathbf{e}_{\mathbf{b}\lambda} = \mathbf{C}_\lambda \cdot \mathbf{q}_\lambda + \mathbf{h}_{\mathbf{o}\lambda}^{s}, \tag{7.3}$$

where $\mathbf{A}_\lambda$, $\mathbf{e}_{\mathbf{b}\lambda}$, $\mathbf{C}_\lambda$, $\mathbf{q}_\lambda$, and $\mathbf{h}_{\mathbf{o}\lambda}^{s}$ are defined as in Chapter 6, but on a spectral basis. Assuming that all the q_j are unknown (and all temperatures are known), equation (7.3) may be solved and integrated as

$$\mathbf{q} = \int_0^\infty \mathbf{q}_\lambda\, d\lambda = \int_0^\infty \mathbf{C}_\lambda^{-1} \cdot [\mathbf{A}_\lambda \cdot \mathbf{e}_{\mathbf{b}\lambda} - \mathbf{h}_{\mathbf{o}\lambda}^{s}]\, d\lambda. \tag{7.4}$$

A similar expression may be found if the heat flux is specified over some of the surfaces (with temperatures unknown). Branstetter [1] carried out integration of equation (7.4) for two infinite, parallel plates with platinum surfaces. In practice, accurate numerical evaluation of equation (7.4) is considered too complicated for most applications: For every wavelength used in the numerical integration (or *quadrature*) the matrix $\mathbf{C}$ needs to be inverted, which—for large numbers of nodes—is generally done by iteration. In addition, if one or more of the surfaces are specular reflectors, the specular view factors need to be recalculated for each wavelength (though not the diffuse view factors of which they are composed). Therefore, nongray effects are usually addressed by simplified models such as the *semigray approximation* or the *band approximation*.

Semigray Approximation

In some applications there is a natural division of the radiative energy within an enclosure into two or more distinct spectral regions. For example, in a solar collector the incoming energy comes from a high-temperature source with most of its energy below 3 μm, while radiation losses

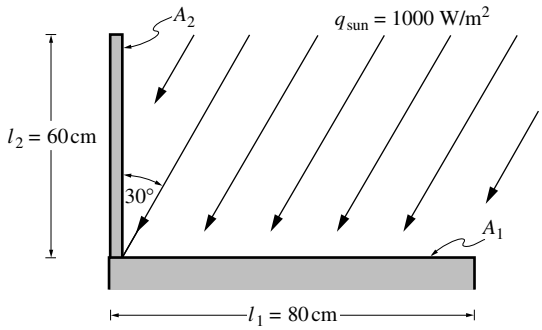

FIGURE 7-1
Solar collector geometry for Example 7.1.

for typical collector temperatures are at wavelengths above 3 μm. In the case of laser heating and processing the incoming energy is monochromatic (at the laser wavelength), while reradiation takes place over the entire near- to midinfrared (depending on the workpiece temperature), etc. In such a situation equation (6.22) may be split into two sets of N equations each, one set for each spectral range, and with different radiative properties for each set. For example, consider an enclosure subject to external irradiation, which is confined to a certain spectral range "(1)". The surfaces in the enclosure, owing to their temperature, emit over spectral range "(2)".[1] Then from equation (6.22),

$$\sum_{j=1}^{N}\left[\frac{\delta_{ij}}{\epsilon_j^{(1)}} - \frac{\rho_j^{d(1)}}{\epsilon_j^{(1)}}F_{i-j}^{s(1)}\right]q_j^{(1)} + H_{oi}^{s} = 0, \tag{7.5a}$$

$$\sum_{j=1}^{N}\left[\frac{\delta_{ij}}{\epsilon_j^{(2)}} - \frac{\rho_j^{d(2)}}{\epsilon_j^{(2)}}F_{i-j}^{s(2)}\right]q_j^{(2)} = \sum_{j=1}^{N}\left[\delta_{ij} - (1-\rho_j^{s(2)})F_{i-j}^{s(2)}\right]E_{bj}, \tag{7.5b}$$

$$q_i = q_i^{(1)} + q_i^{(2)}, \qquad i = 1, 2, \ldots, N, \tag{7.5c}$$

where $\epsilon_j^{(1)}$ is the average emittance for surface j over spectral interval (1), and so on.

Example 7.1. A very long solar collector plate is to collect energy at a temperature of $T_1 = 350\,K$. To improve its performance for off-normal solar incidence, a surface, which is highly reflective at short wavelengths, is placed next to the collector as shown in Fig. 7-1. For simplicity you may make the following assumptions: (*i*) The collector A_1 is isothermal and a diffuse reflector; (*ii*) the mirror A_2 is a specular reflector; (*iii*) the spectral properties of the collector and mirror may be approximated as

$$\epsilon_1 = 1 - \rho_1^d = \begin{cases} 0.8, & \lambda < \lambda_c = 4\,\mu m, \\ 0.1, & \lambda > \lambda_c, \end{cases}$$

$$\epsilon_2 = 1 - \rho_2^s = \begin{cases} 0.1, & \lambda < \lambda_c, \\ 0.8, & \lambda > \lambda_c, \end{cases}$$

and (*iv*) heat losses from the mirror by convection as well as all losses from the collector ends may be neglected. How much energy (per unit length) does the collector plate collect for a solar incidence angle of 30°?

Solution
From equation (7.5) we find, with $F_{1-2}^s = F_{1-2}$, $F_{2-1}^s, = F_{2-1}$, and $F_{1-1}^s = F_{2-2}^s = 0$, for range (1),

$$\frac{q_1^{(1)}}{\epsilon_1^{(1)}} + H_{o1}^s = 0,$$

$$-\left(\frac{1}{\epsilon_1^{(1)}} - 1\right)F_{2-1}q_1^{(1)} + \frac{q_2^{(1)}}{\epsilon_2^{(1)}} + H_{o2}^s = 0,$$

and for range (2),

[1]Note that spectral ranges "(1)" and "(2)" do not need to cover the entire spectrum and, indeed, they may overlap.

$$\frac{q_1^{(2)}}{\epsilon_1^{(2)}} = E_{b1} - \epsilon_2^{(2)} F_{1-2} E_{b2},$$

$$-\left(\frac{1}{\epsilon_1^{(2)}} - 1\right) F_{2-1} q_1^{(2)} + \frac{q_2^{(2)}}{\epsilon_2^{(2)}} = -F_{2-1} E_{b1} + E_{b2}.$$

Eliminating E_{b2} from the last two equations, we find

$$\left[\frac{1}{\epsilon_1^{(2)}} - \left(\frac{1}{\epsilon_1^{(2)}} - 1\right)\epsilon_2^{(2)} F_{1-2} F_{2-1}\right] q_1^{(2)} + F_{1-2} q_2^{(2)} = (1 - \epsilon_2^{(2)} F_{1-2} F_{2-1}) E_{b1}.$$

Multiplying the second equation for range (1) by $\epsilon_2^{(1)} F_{1-2}$ results in

$$-\left(\frac{1}{\epsilon_1^{(1)}} - 1\right)\epsilon_2^{(1)} F_{1-2} F_{2-1} q_1^{(1)} + F_{1-2} q_2^{(1)} = -\epsilon_2^{(1)} F_{1-2} H_{o2}^s.$$

Adding the last two equations and using $q_2 = q_2^{(1)} + q_2^{(2)} = 0$ then leads to

$$\left[\frac{1}{\epsilon_1^{(2)}} - \left(\frac{1}{\epsilon_1^{(2)}} - 1\right)\epsilon_2^{(2)} F_{1-2} F_{2-1}\right] q_1^{(2)} = \left(\frac{1}{\epsilon_1^{(1)}} - 1\right)\epsilon_2^{(1)} F_{1-2} F_{2-1} q_1^{(1)} - \epsilon_2^{(1)} F_{1-2} H_{o2}^s + \left(1 - \epsilon_2^{(2)} F_{1-2} F_{2-1}\right) E_{b1},$$

or, with $q_1^{(1)} = -\epsilon_1^{(1)} H_{o1}^s$,

$$q_1 = q_1^{(1)} + q_1^{(2)} = \frac{(1-\epsilon_2^{(2)} F_{1-2} F_{2-1}) E_{b1} - (1-\epsilon_1^{(1)})\epsilon_2^{(1)} F_{1-2} F_{2-1} H_{o1}^s - \epsilon_2^{(1)} F_{1-2} H_{o2}^s}{1/\epsilon_1^{(2)} - \left(1/\epsilon_1^{(2)} - 1\right)\epsilon_2^{(2)} F_{1-2} F_{2-1}} - \epsilon_1^{(1)} H_{o1}^s.$$

From Example 6.5 we have

$$H_{o2}^s = q_{\text{sun}} \sin\varphi = 1000 \times \sin 30^\circ = 500\,\text{W/m}^2,$$

$$H_{o1}^s = q_{\text{sun}} \left[\cos\varphi + \rho_2^{s(1)} \sin\varphi\,(l_2/l_1)\right] = 1000\,[\cos 30^\circ + 0.9 \times \sin 30^\circ (60/80)] = 1203.5\,\text{W/m}^2.$$

With $F_{1-2} = \frac{1}{4}$, $F_{2-1} = \frac{1}{3}$, $F_{1-2}F_{2-1} = \frac{1}{12}$, and $E_{b1} = 5.670 \times 10^{-8} \times 350^4 = 850.9\,\text{W/m}^2$, q_1 may now be evaluated as

$$q_1 = \frac{\left(1 - \frac{0.8}{12}\right) \times 850.9 - \frac{0.2 \times 0.1}{12} \times 1203.5 - \frac{0.1}{4} \times 500}{\frac{1}{0.1} - \left(\frac{1}{0.1} - 1\right) \times \frac{0.8}{12}} - 0.8 \times 1203.5 = 82.9 - 962.8 = -880.1\,\text{W/m}^2,$$

or a collection efficiency of 88%! In addition, surface A_2 remains much cooler than for the gray case (Example 6.5); from the first equation for region (2)

$$E_{b2} = \left(E_{b1} - \frac{q_1^{(2)}}{\epsilon_1^{(2)}}\right) \Big/ \epsilon_2^{(2)} F_{1-2} = \left(850.9 - \frac{82.9}{0.1}\right) \Big/ \frac{0.8}{4} = 109.5\,\text{W/m}^2,$$

or

$$T_2 = (E_{b2}/\sigma)^{1/4} = \left[109.5/5.670 \times 10^{-8}\right]^{1/4} = 209\,\text{K}.$$

Obviously, surface A_2 would heat up by convection from the surroundings. Surface emission from A_2 would then further improve the collection efficiency.

Thus, selective surfaces can have enormous impact on radiative heat fluxes in configurations with irradiation from high-temperature sources. Subroutine `semigray` is provided in Appendix F for the solution of the simultaneous equations (7.5), requiring surface information and a partial view factor matrix as input (i.e., the code is limited to two spectral ranges, separating external irradiation from surface emission). The solution to Example 7.1 is also given in the form of program `semigrxch`, which may be used as a starting point for the solution to other problems. Fortran90, C++ as well as MATLAB® versions are provided.

The semigray approximation is not limited to two distinct spectral regions. Each surface of the enclosure may be given a set of absorptances and reflectances, one value for each different surface temperature (with its different emission spectra). Armaly and Tien [2] have indicated

how such absorptances may be determined. However, while simple and straightforward, the method can never become "exact," no matter how many different values of absorptance and reflectance are chosen for each surface.

Bobco and coworkers [3] have given a general discussion of the semigray approximation. The method has been applied to solar irradiation falling into a V-groove cavity with a spectrally selective, diffusely reflecting surface by Plamondon and Landram [4]. Comparison with exact (i.e., spectrally integrated) results proved the method to be very accurate. Shimoji [5] used the semigray approximation to model solar irradiation onto conical and V-groove cavities whose reflectances had purely diffuse and specular components.

Band Approximation

Another commonly used method of solving equation (7.1) is the *band approximation*. In this method the spectrum is broken up into M bands, over which the radiative properties of *all* surfaces in the enclosure are constant. Therefore,

$$\sum_{j=1}^{N}\left[\delta_{ij}-(1-\rho_j^{s(m)})F_{i-j}^{s(m)}\right]E_{bj}^{(m)} = \sum_{j=1}^{N}\left[\frac{\delta_{ij}}{\epsilon_j^{(m)}}-\frac{\rho_j^{d(m)}}{\epsilon_j^{(m)}}F_{i-j}^{s(m)}\right]q_j^{(m)}+H_{oi}^{s(m)},$$
$$i=1,2,\ldots,N,\quad m=1,2,\ldots,M; \tag{7.6a}$$

$$E_{bj}=\sum_{m=1}^{M}E_{bj}^{(m)},\quad q_j=\sum_{m=1}^{M}q_j^{(m)},\quad H_{oi}^{s}=\sum_{m=1}^{M}H_{oi}^{s(m)}. \tag{7.6b}$$

Equation (7.6) is, of course, nothing but a simple numerical integration of equation (7.1), using the trapezoidal rule with varying steps. This method has the advantage that the widths of the bands can be tailored to the spectral variation of properties, resulting in good accuracy with relatively few bands. For very few bands the accuracy of this method is similar to that of the semigray approximation, but is a little more cumbersome to apply, and requires an iterative approach if some surfaces have prescribed radiative flux rather than temperature. On the other hand, the *band approximation* can achieve any desired accuracy by using many bands.

Example 7.2. Repeat Example 7.1 using the band approximation.

Solution

Since the emittances in this example have been idealized to have constant values across the spectrum with the exception of a step at $\lambda = 4\,\mu$m, a two-band approximation ($\lambda < \lambda_c = 4\,\mu$m and $\lambda > 4\,\mu$m) will produce the "exact" solution (within the framework of the net radiation method). From equation (7.6)

$$E_{b1}^{(m)}-\epsilon_2^{(m)}F_{1-2}E_{b2}^{(m)} = \frac{q_1^{(m)}}{\epsilon_1^{(m)}}+H_{o1}^{s(m)},$$
$$-F_{2-1}E_{b1}^{(m)}+E_{b2}^{(m)} = -\left(\frac{1}{\epsilon_1^{(m)}}-1\right)F_{2-1}q_1^{(m)}+\frac{q_2^{(m)}}{\epsilon_2^{(m)}}+H_{o2}^{s(m)},\quad m=1,2,$$

where $E_{bi}^{(1)}=\int_0^{\lambda_c}E_{b\lambda i}\,d\lambda = f(\lambda_c T_i)E_{bi}$, $E_{bi}^{(2)}=[1-f(\lambda_c T_i)]\,E_{bi}$, etc. These are four equations in the six unknowns $q_1^{(m)}$, $q_2^{(m)}$, $E_{b2}^{(m)}$, $m=1,2$. Two more conditions are obtained from $q_2=q_2^{(1)}+q_2^{(2)}=0$ and $E_{b2}^{(1)}+E_{b2}^{(2)}=E_{b2}=\sigma T_2^4$. The problem is that $E_{b2}^{(m)}$ are nonlinear relations in T_2, making it impossible to find explicit relations for the desired $q_1=q_1^{(1)}+q_1^{(2)}$. The system is solved by iteration, by solving for $q_i^{(m)}$:

$$q_1^{(m)}=\epsilon_1^{(m)}\left(E_{b1}^{(m)}-\epsilon_2^{(m)}F_{1-2}E_{b2}^{(m)}-H_{o1}^{s(m)}\right),$$
$$q_2^{(m)}=\epsilon_2^{(m)}\left[\left(\frac{1}{\epsilon_1^{(m)}}-1\right)F_{2-1}q_1^{(m)}-F_{2-1}E_{b1}^{(m)}+E_{b2}^{(m)}-H_{o2}^{s(m)}\right],\quad m=1,2.$$

First, T_2 is guessed, from which the $E_{b2}^{(m)}$ may be evaluated. This computation is followed by determining the $q_1^{(m)}$, after which the $q_2^{(m)}$ can be calculated. If $q_2 > 0$, surface A_2 is too hot and its temperature is reduced and vice versa until the correct temperature is obtained. This calculation may be done by writing a simple computer code, resulting in $T_2 = 212\,\text{K}$ and $q_1 = -867\,\text{W/m}^2$. As expected, for the present example the band approximation offers little improvement while complicating the analysis. However, the band approximation is the method of choice if no distinct spectral regions are obvious and/or the spectral behavior of properties is more involved.

Subroutine `bandapp` is provided in Appendix F for the solution of the simultaneous equations (7.6), requiring surface information and a partial view factor matrix as input. The solution to Example 7.2 is also given in the form of a program `bandmxch`, which may be used as a starting point for the solution to other problems. Fortran90, C++ as well as MATLAB® versions are provided. Dunkle and Bevans [6] applied the band approximation to the same problem as Branstetter [1] (infinite, parallel, tungsten plates) as well as to some other configurations, showing that the band approximation generally achieves accuracies of 2% and better with very few bands, while a gray analysis may result in errors of 30% or more.

7.3 DIRECTIONALLY NONIDEAL SURFACES

In the vast majority of applications the assumption of "directionally ideal" surfaces gives results of sufficient accuracy, i.e., surfaces may be assumed to be diffusely emitting and absorbing and to be diffusely and/or specularly reflecting (with the magnitude of reflectance independent of incoming direction). However, that these results are not always accurate and that heat fluxes are not necessarily bracketed by the diffuse- and specular-reflection cases have been shown in Fig. 6-17 for V-grooves. There will be situations where (*i*) the directional properties, (*ii*) the geometrical considerations, and/or (*iii*) the accuracy requirements are such that the directional behavior of radiation properties must be addressed.

If radiative properties with arbitrary directional behavior are to be accounted for, it is no longer possible to reduce the governing equation to an integral equation in a single quantity (the radiosity) that is a function of surface location only (but not of direction). Rather, applying conservation of energy to this problem produces an equation governing the directional intensity leaving a surface that is a function of both location on the enclosure surface and direction.

The Governing Equation for Intensity

Consider the arbitrary enclosure shown in Fig. 7-2. The spectral radiative heat flux leaving an infinitesimal surface element dA' into the direction of $\hat{\mathbf{s}}'$ and arriving at surface element dA is

$$I_\lambda(\mathbf{r}', \lambda, \hat{\mathbf{s}}')\, dA'_p\, d\Omega = I_\lambda(\mathbf{r}', \lambda, \hat{\mathbf{s}}')(dA' \cos\theta')\frac{dA\cos\theta_i}{S^2}, \tag{7.7}$$

where $S = |\mathbf{r}' - \mathbf{r}|$ is the distance between dA' and dA, $\cos\theta' = \hat{\mathbf{s}}' \cdot \hat{\mathbf{n}}'$ is the cosine of the angle between the unit direction vector $\hat{\mathbf{s}}' = (\mathbf{r} - \mathbf{r}')/S$ and the outward surface normal $\hat{\mathbf{n}}'$ at dA' and, similarly, $\cos\theta_i = (-\hat{\mathbf{s}}') \cdot \hat{\mathbf{n}}$ at dA. This irradiation at dA coming from dA' may also be expressed, from equation (3.32), as

$$H'_\lambda(\mathbf{r}, \lambda, \hat{\mathbf{s}}')\, dA\, d\Omega_i = I_\lambda(\mathbf{r}, \lambda, \hat{\mathbf{s}}')\, dA \cos\theta_i\, \frac{dA'\cos\theta'}{S^2}. \tag{7.8}$$

Equating these two expressions, we find

$$I_\lambda(\mathbf{r}, \lambda, \hat{\mathbf{s}}') = I_\lambda(\mathbf{r}', \lambda, \hat{\mathbf{s}}'), \tag{7.9}$$

that is, the radiative intensity remains unchanged as it travels from dA' to dA.

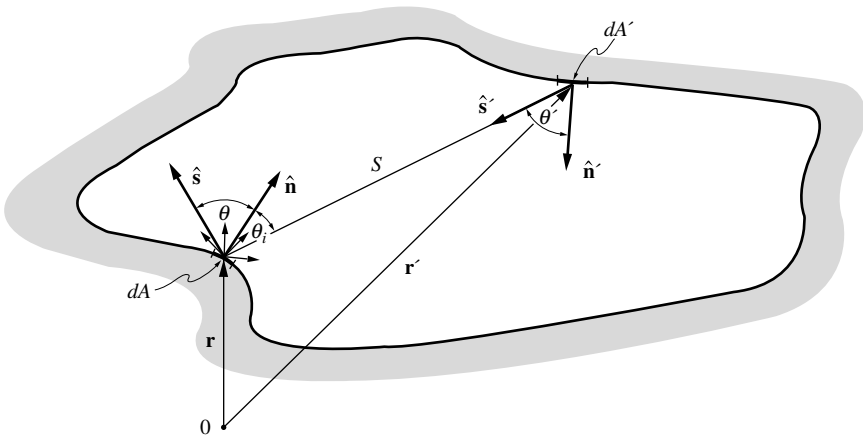

FIGURE 7-2
Radiative exchange in an enclosure with arbitrary surface properties.

The outgoing intensity at dA into the direction of $\hat{\mathbf{s}}$ consists of two contributions: locally emitted intensity and reflected intensity. The locally emitted intensity is, from equation (3.1),

$$\epsilon'_\lambda(\mathbf{r}, \lambda, \hat{\mathbf{s}}) I_{b\lambda}(\mathbf{r}, \lambda).$$

The amount of irradiation at dA coming from dA' [equation (7.8)] that is reflected into a solid angle $d\Omega_o$ around the direction $\hat{\mathbf{s}}$ is, from the definition of the bidirectional reflection function, equation (3.33),

$$dI_\lambda(\mathbf{r}, \lambda, \hat{\mathbf{s}})\, d\Omega_o = \rho''_\lambda(\mathbf{r}, \lambda, \hat{\mathbf{s}}', \hat{\mathbf{s}}) \left(H'_\lambda(\mathbf{r}, \lambda, \hat{\mathbf{s}}')\, d\Omega_i \right) d\Omega_o,$$

or

$$\begin{aligned} dI_\lambda(\mathbf{r}, \lambda, \hat{\mathbf{s}}) &= \rho''_\lambda(\mathbf{r}, \lambda, \hat{\mathbf{s}}', \hat{\mathbf{s}}) I_\lambda(\mathbf{r}, \lambda, \hat{\mathbf{s}}') \cos\theta_i\, d\Omega_i \\ &= \rho''_\lambda(\mathbf{r}, \lambda, \hat{\mathbf{s}}', \hat{\mathbf{s}}) I_\lambda(\mathbf{r}, \lambda, \hat{\mathbf{s}}') \frac{\cos\theta_i \cos\theta'}{S^2}\, dA'. \end{aligned}$$

Integrating the reflected intensity over all incoming directions (or over the entire enclosure surface), and adding the locally emitted intensity, we find an expression for the outgoing intensity at dA as

$$\begin{aligned} I_\lambda(\mathbf{r}, \lambda, \hat{\mathbf{s}}) &= \epsilon'_\lambda(\mathbf{r}, \lambda, \hat{\mathbf{s}}) I_{b\lambda}(\mathbf{r}, \lambda) + \int_{2\pi} \rho''_\lambda(\mathbf{r}, \lambda, \hat{\mathbf{s}}', \hat{\mathbf{s}}) I_\lambda(\mathbf{r}', \lambda, \hat{\mathbf{s}}') \cos\theta_i\, d\Omega_i \\ &= \epsilon'_\lambda(\mathbf{r}, \lambda, \hat{\mathbf{s}}) I_{b\lambda}(\mathbf{r}, \lambda) + \int_A \rho''_\lambda(\mathbf{r}, \lambda, \hat{\mathbf{s}}', \hat{\mathbf{s}}) I_\lambda(\mathbf{r}', \lambda, \hat{\mathbf{s}}') \frac{\cos\theta_i \cos\theta'}{S^2}\, dA'. \end{aligned} \tag{7.10}$$

Equation (7.10) is an integral equation for outgoing intensity ($\hat{\mathbf{n}} \cdot \hat{\mathbf{s}} > 0$) anywhere on the surface enclosure. Once a solution to equation (7.10) has been obtained (analytically, numerically, or statistically; approximately or "exactly"), the net radiative heat flux is determined from

$$\begin{aligned} q_\lambda(\mathbf{r}, \lambda) &= q_{\text{out}} - q_{\text{in}} \\ &= \int_{\hat{\mathbf{n}}\cdot\hat{\mathbf{s}}>0} I_\lambda(\mathbf{r}, \lambda, \hat{\mathbf{s}}) \cos\theta\, d\Omega - \int_{\hat{\mathbf{n}}\cdot\hat{\mathbf{s}}<0} I_\lambda(\mathbf{r}, \lambda, \hat{\mathbf{s}}') \cos\theta_i\, d\Omega_i \\ &= \int_{\hat{\mathbf{n}}\cdot\hat{\mathbf{s}}>0} I_\lambda(\mathbf{r}, \lambda, \hat{\mathbf{s}}) \cos\theta\, d\Omega - \int_A I_\lambda(\mathbf{r}', \lambda, \hat{\mathbf{s}}') \frac{\cos\theta_i \cos\theta'}{S^2}\, dA', \end{aligned} \tag{7.11}$$

or, equivalently, from

$$q_\lambda(\mathbf{r},\lambda) = q_{\text{em}} - q_{\text{abs}} = \epsilon_\lambda E_{b\lambda} - \alpha_\lambda H_\lambda$$
$$= \int_{\hat{\mathbf{n}}\cdot\hat{\mathbf{s}}>0} \epsilon'_\lambda(\mathbf{r},\lambda,\hat{\mathbf{s}})\cos\theta\, d\Omega\, I_{b\lambda}(\mathbf{r},\lambda) - \int_A \alpha'_\lambda(\mathbf{r},\lambda,\hat{\mathbf{s}}')I_\lambda(\mathbf{r}',\lambda,\hat{\mathbf{s}}')\frac{\cos\theta_i\cos\theta'}{S^2}\,dA'. \quad (7.12)$$

Both forms of equation (7.10) (solid angle and area integration) may be employed, depending on the problem at hand. For example, if dA is a diffuse emitter and reflector then, from equation (3.38), $\rho''_\lambda(\mathbf{r},\lambda,\hat{\mathbf{s}}',\hat{\mathbf{s}}) = \rho'_\lambda(\mathbf{r},\lambda)/\pi$ and, from equation (5.19), $I_\lambda(\mathbf{r},\lambda,\hat{\mathbf{s}}) = J_\lambda(\mathbf{r},\lambda)/\pi$. If dA' is also diffuse, we obtain from the second form of equation (7.10)

$$J_\lambda(\mathbf{r},\lambda) = \epsilon_\lambda(\mathbf{r},\lambda)E_{b\lambda}(\mathbf{r},\lambda) + \rho_\lambda(\mathbf{r},\lambda)\int_A J_\lambda(\mathbf{r}',\lambda)\,dF_{dA-dA'}, \quad (7.13)$$

which is nothing but the spectral form of equation (5.24) without external irradiation.[2] Similarly, equation (7.11) reduces to

$$q_\lambda(\mathbf{r},\lambda) = J_\lambda(\mathbf{r},\lambda) - \int_A J_\lambda(\mathbf{r}',\lambda)\,dF_{dA-dA'}, \quad (7.14)$$

the spectral form of equation (5.25).

On the other hand, if dA is a specular reflector the first form of equation (7.10) becomes more convenient: For a specular surface we have $\rho''_\lambda = 0$ for all $\hat{\mathbf{s}}'$ except for $\hat{\mathbf{s}}' = \hat{\mathbf{s}}_s$, where $\hat{\mathbf{s}}_s$ is the "specular direction" from which a beam must originate in order to travel on into the direction of $\hat{\mathbf{s}}$ after specular reflection. For that direction $\rho''_\lambda \to \infty$, and it is clear that the integrand of the integral in equation (7.10) will be nonzero only in the immediate vicinity of $\hat{\mathbf{s}}' = \hat{\mathbf{s}}_s$. In that vicinity $I_\lambda(\mathbf{r}',\lambda,\hat{\mathbf{s}}')$ varies very little and we may remove it from the integral. From the definition of the spectral, directional–hemispherical reflectance, equation (3.37), and the law of reciprocity for the bidirectional reflectance function, equation (3.35), we obtain

$$\int_{2\pi}\rho''_\lambda(\mathbf{r},\lambda,\hat{\mathbf{s}}',\hat{\mathbf{s}})I_\lambda(\mathbf{r},\lambda,\hat{\mathbf{s}}')\cos\theta_i\,d\Omega_i = I_\lambda(\mathbf{r}',\lambda,\hat{\mathbf{s}}_s)\int_{2\pi}\rho''_\lambda(\mathbf{r},\lambda,\hat{\mathbf{s}}',\hat{\mathbf{s}})\cos\theta_i\,d\Omega_i$$
$$= I_\lambda(\mathbf{r}',\lambda,\hat{\mathbf{s}}_s)\int_{2\pi}\rho''_\lambda(\mathbf{r},\lambda,-\hat{\mathbf{s}},-\hat{\mathbf{s}}')\cos\theta_i\,d\Omega_i$$
$$= I_\lambda(\mathbf{r}',\lambda,\hat{\mathbf{s}}_s)\rho'_\lambda(\mathbf{r},\lambda,-\hat{\mathbf{s}}),$$

where $-\hat{\mathbf{s}}$ denotes an incoming direction, pointing toward dA, and $\rho'_\lambda(\mathbf{r},\lambda,-\hat{\mathbf{s}})$ is the directional–hemispherical reflectance. From the same Kirchhoff's law used to establish equation (3.35), it follows that $\rho'_\lambda(\mathbf{r},\lambda,-\hat{\mathbf{s}}) = \rho'_\lambda(\mathbf{r},\lambda,\hat{\mathbf{s}}_s)$ and

$$I_\lambda(\mathbf{r},\lambda,\hat{\mathbf{s}}) = \epsilon'_\lambda(\mathbf{r},\lambda,\hat{\mathbf{s}})I_{b\lambda}(\mathbf{r},\lambda) + \rho'_\lambda(\mathbf{r},\lambda,\hat{\mathbf{s}}_s)I_\lambda(\mathbf{r}',\lambda,\hat{\mathbf{s}}_s). \quad (7.15)$$

Example 7.3. Consider a very long V-groove with an opening angle of $2\gamma = 90°$ and with optically smooth metallic surfaces with index of refraction $m = n - ik = 23.452(1-i)$, i.e., the surfaces are specularly reflecting and their directional dependence obeys Fresnel's equations. The groove is isothermal at temperature T, and no external irradiation is entering the configuration. Calculate the local net radiative heat loss as a function of the distance from the vertex of the groove.

Solution

This is one of the problems studied by Toor [7], using the Monte Carlo method (the solid line in Fig. 6-17). The directional emittance may be calculated from Fresnel's equations for a metal, equations (3.75) and (3.76), as

$$\epsilon'(\theta) = 1 - \rho'(\theta) = \frac{2n\cos\theta}{(n+\cos\theta)^2 + k^2} + \frac{2n\cos\theta}{(n\cos\theta+1)^2 + (k\cos\theta)^2},$$

[2] External irradiation is readily included in equations (7.10) and (7.11) by replacing I_λ with $I_\lambda + I_{o\lambda}$ inside the integrals.

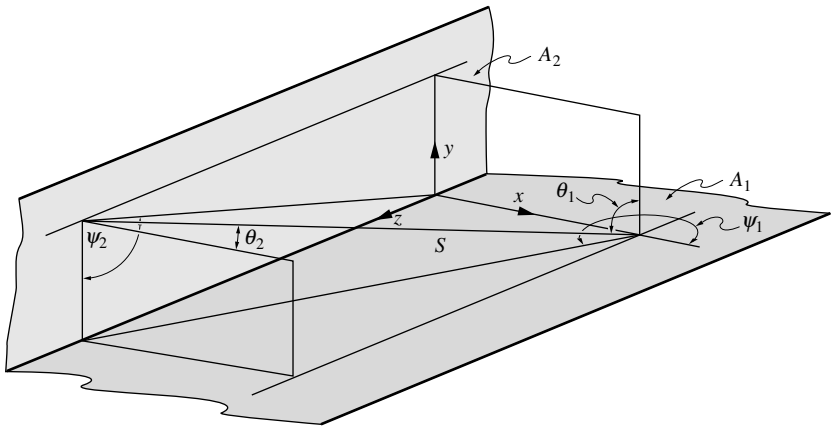

FIGURE 7-3
Isothermal V-groove with specularly reflecting, directionally dependent reflectance (Example 7.3).

while the hemispherical emittance follows from equation (3.77) or Fig. 3-10 as $\epsilon = 0.1$.

The present problem is particularly simple since the surfaces are specular reflectors and since the opening angle of the groove is 90° (cf. Fig. 7-3). Any radiation leaving surface A_1 traveling toward A_2 will be absorbed by A_2 or reflected out of the groove; none can be reflected back to A_1. This fact implies that all radiation arriving at A_1 is due to emission from A_2, which is a known quantity. Therefore, for those azimuthal angles ψ_2 pointing toward A_1 we have

$$-\frac{\pi}{2} < \psi_2 < \frac{\pi}{2}: \qquad I_2(\theta_2) = \epsilon'(\theta_2) I_b,$$

and the local heat flux follows from equation (7.12) as

$$\begin{aligned} q(x) &= \epsilon E_b - \int_{2\pi} \epsilon'(\theta_1) I_2(\theta_2) \cos\theta_1 \, d\Omega_1 \\ &= \epsilon E_b - 2 \int_{\psi_1=0}^{\pi/2} \int_{\theta_1=\theta_{1\min}(\psi_1)}^{\pi/2} \epsilon'(\theta_1)\epsilon'(\theta_2) I_b \cos\theta_1 \sin\theta_1 \, d\theta_1 \, d\psi_1, \end{aligned}$$

or

$$\frac{q(x)}{\epsilon E_b} = 1 - \frac{2}{\pi\epsilon} \int_{\psi_1=0}^{\pi/2} \int_{\theta_1=\theta_{1\min}(\psi_1)}^{\pi/2} \epsilon'(\theta_1)\epsilon'(\theta_2) \cos\theta_1 \sin\theta_1 \, d\theta_1 \, d\psi_1.$$

Here the limits on the integral express the fact that the solid angle, with which A_2 is seen from A_1, is limited. It remains to express $\theta_{1\min}$ as well as θ_2 in terms of θ_1 and ψ_1. From Fig. 7-3 it follows that

$$\cos\theta_1 = \frac{y}{S}, \quad \cos\theta_2 = \frac{x}{S}, \quad S\sin\theta_1 = \frac{x}{\cos\psi_1}.$$

From these three relations and the fact that the minimum value of θ_1 occurs when $y = L$, we find

$$\cos\theta_2 = \sin\theta_1 \cos\psi_1 \quad \text{and} \quad \theta_{1\min}(\psi_1) = \tan^{-1}\frac{x}{L\cos\psi_1}.$$

Using Fresnel's equation for the directional emittance, the nondimensional local heat flux $q(x)/\epsilon E_b$ may now be calculated using numerical integration. The resulting heat flux is shown as the solid line in Fig. 6-17. This result should be compared with the simpler case of diffuse emission, or $\epsilon'(\theta) = \epsilon = 0.1 = \text{const}$. For that case the integral above is readily integrated analytically, resulting in the dash-dotted line of Fig. 6-17. The two results are very close, with a maximum error of $\simeq 2\%$ near the vertex of the groove.

While the evaluation of the "exact" heat flux, using Fresnel's equations, was quite straightforward in this very simple problem, these calculations are normally much, much more involved than the diffuse-emission approximation. Before embarking on such extensive calculations it is important to ask oneself whether employing Fresnel's equations will lead to substantially different results for the problem at hand.

Few numerical solutions of the exact integral equations have appeared in the literature. For example, Hering and Smith [8] considered the same problem as Example 7.3, but for varying opening angles and for rough surface materials (with the bidirectional reflection function as given in an earlier paper [9]). Lack of detailed knowledge of bidirectional reflection distributions, as well as the enormous complexity involved in the solution of the integral equation (7.10), makes it necessary in practice to make additional simplifying assumptions or to employ a different approach, such as the Monte Carlo method (to be discussed in Chapter 8).

Net Radiation Method

It is possible to apply the net radiation method to surfaces with directionally nonideal properties, although its application is considerably more difficult and restrictive. Breaking up the enclosure into N subsurfaces we may write equation (7.10), for $\mathbf{r}$ pointing to a location on subsurface A_i, as

$$I(\mathbf{r}, \lambda, \hat{\mathbf{s}}) = \epsilon'(\mathbf{r}, \lambda, \hat{\mathbf{s}}) I_b(\mathbf{r}, \lambda) + \pi \sum_{j=1}^{N} \rho_j''(\mathbf{r}, \lambda, \hat{\mathbf{s}}) I_j(\mathbf{r}, \lambda) F_{di-j}(\mathbf{r}), \tag{7.16}$$

where we have dropped the subscript λ for simplicity of notation, and where ρ_j'' and I_j are "suitable" average values between point $\mathbf{r}$ and surface A_j. Averaging equation (7.16) over A_i leads to

$$I_i(\lambda, \hat{\mathbf{s}}) = \epsilon_i'(\lambda, \hat{\mathbf{s}}) I_{bi}(\lambda) + \pi \sum_{j=1}^{N} \rho_{ji}'(\lambda, \hat{\mathbf{s}}) I_{ji}(\lambda) F_{i-j}, \quad i = 1, 2, \ldots, N. \tag{7.17}$$

Here I_{ji} is an average value of the intensity leaving surface A_j traveling toward A_i, and ρ_{ji}' is a corresponding value for the bidirectional reflection function. If we assume that the enclosure temperature and surface properties are known everywhere, then equation (7.17) has N unknown intensities I_{ji} ($j = 1, 2, \ldots, N$) for each subsurface A_i. Thus, if equation (7.17) is averaged over all the solid angles with which subsurface A_k is seen from A_i, it becomes a set of $N \times N$ equations in the N^2 unknown I_{ik}:

$$I_{ik}(\lambda) = \epsilon_{ik}(\lambda) I_{bi}(\lambda) + \pi \sum_{j=1}^{N} \rho_{jik}(\lambda) I_{ji}(\lambda) F_{i-j}, \quad i, k = 1, 2, \ldots, N. \tag{7.18}$$

Here ρ_{jik} is an average value of the bidirectional reflection function for radiation traveling from A_j to A_k via reflection at A_i. For a diffusely emitting, absorbing, and reflecting enclosure we have $\epsilon_{ik} = \epsilon_i$, $\pi \rho_{jik} = \rho_i$, and equation (7.18) becomes, with $I_{ji} = I_j = J_j/\pi$,

$$J_i = \epsilon_i E_{bi} + \rho_i \sum_{j=1}^{N} J_j F_{i-j}, \quad i = 1, 2, \ldots, N, \tag{7.19}$$

which is identical to equations (5.30) and (5.31) (without external irradiation).

If the N subsurfaces are relatively small (as compared with the distance-squared between them), average properties ϵ_{ik} and ρ_{jik} may be obtained simply by evaluating ϵ' and ρ'' at the directions given by connecting the centerpoints of surface A_i with A_j and A_k. For larger subsurfaces a more elaborate averaging may be desirable. A discussion on that subject has been given by Bevans and Edwards [10].

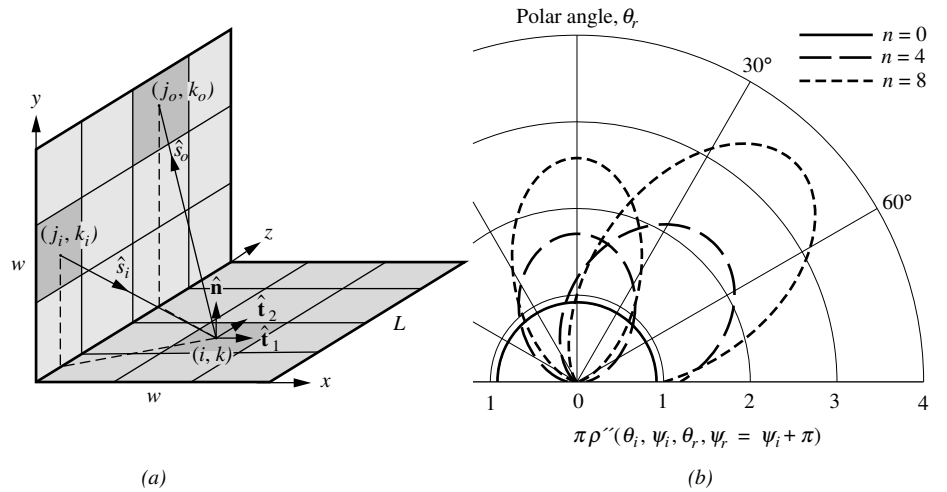

FIGURE 7-4
(*a*) Geometry for Example 7.4, (*b*) bidirectional reflection function in plane of incidence for $\theta_i = 0°$ and $\theta_i = 45°$, for the material of Example 7.4.

Once the N^2 unknown I_{ik} have been determined, the average heat flux on A_i may be calculated from equations (7.18) and (7.11) or (7.12) as

$$q_i(\lambda) = \pi \sum_{k=1}^{N} I_{ik}(\lambda) F_{i-k} - \pi \sum_{j=1}^{N} I_{ji}(\lambda) F_{i-j} = \pi \sum_{j=1}^{N} (I_{ij} - I_{ji}) F_{i-j} \tag{7.20a}$$

$$= \epsilon_i(\lambda) E_{bi}(\lambda) - \pi \sum_{j=1}^{N} \alpha_{ij}(\lambda) I_{ji}(\lambda) F_{i-j}, \quad i = 1, 2, \ldots, N, \tag{7.20b}$$

where ϵ_i is the hemispherical emittance of A_i and α_{ij} is the average absorptance of subsurface A_i for radiation coming from A_j.

It is apparent from equations (7.10) and (7.18) that the net radiation method for directionally nonideal surfaces is valid (*i*) if each I_{bi} varies little over each subsurface A_i, (*ii*) if each I_{ik} varies little between any two positions on A_i and A_k, and (*iii*) if similar restrictions apply to ϵ_{ik}, α_{ij}, and ρ_{jik}. Restrictions (*ii*) and (*iii*) are likely to be easily violated unless the surfaces are near-diffuse reflectors or are very small (as compared with the distance between them).

Equations (7.10) and (7.18) are valid for an enclosure with gray surface properties, or on a spectral basis. For nongray surface properties the governing equations are readily integrated over the spectrum using the methods outlined in the previous section.

To illustrate the difficulties associated with directionally nonideal surfaces, we shall consider one particularly simple example.

Example 7.4. Consider the isothermal corner of finite length as depicted in Fig. 7-4*a*. The surface material is similar to the one of the infinitely long corner of the previous example, i.e., the absorptance and emittance obey Fresnel's equations with $m = n - ik = 23.452(1 - i)$, and a hemispherical emittance of $\epsilon = 0.1$. However, in the present example we assume that the material is reflecting in a nonspecular fashion with a bidirectional reflection function of

$$\rho''(\hat{\mathbf{s}}_i, \hat{\mathbf{s}}_r) = \frac{\rho'(\hat{\mathbf{s}}_i)}{\pi C_n(\hat{\mathbf{s}}_i)} (1 + \hat{\mathbf{s}}_s \cdot \hat{\mathbf{s}}_r)^n,$$

where $\hat{\mathbf{s}}_i$ is the direction of incoming radiation, $\hat{\mathbf{s}}_s$ is the specular reflection direction (i.e., $\theta_s = \theta_i$, $\psi_s = \psi_i + \pi$), and $\hat{\mathbf{s}}_r$ is the actual direction of reflection. This form of the bidirectional reflection function describes a surface that has a reflectance maximum in the specular direction, and whose reflectance

drops off equally in all directions away from the specular direction (i.e., with changing polar angle and/or azimuthal angle). Since the directional–hemispherical reflectance must obey $\rho'(\hat{\mathbf{s}}_i) = 1 - \epsilon'(\hat{\mathbf{s}}_i)$, the function $C_n(\hat{\mathbf{s}}_i)$ follows from equation (3.37) as

$$C_n(\hat{\mathbf{s}}_i) = \frac{1}{\pi} \int_{2\pi} (1 + \hat{\mathbf{s}}_s \cdot \hat{\mathbf{s}}_r)^n \cos\theta_r \, d\Omega_r.$$

Determine the local radiative heat loss rates from the plates for the case that both plates are isothermal at the same temperature.

Solution

The direction vectors $\hat{\mathbf{s}}$ may be expressed in terms of polar angle θ and azimuthal angle ψ, or $\hat{\mathbf{s}} = \sin\theta(\cos\psi\hat{\mathbf{t}}_1 + \sin\psi\hat{\mathbf{t}}_2) + \cos\theta\hat{\mathbf{n}}$, where $\hat{\mathbf{n}}$ is the unit surface normal and $\hat{\mathbf{t}}_1$ and $\hat{\mathbf{t}}_2$ are two perpendicular unit vectors tangential to the surface. Therefore, the bidirectional reflection function may be written as

$$\rho''(\theta_i, \psi_i, \theta_r, \psi_r) = \frac{\rho'(\theta_i, \psi_i)}{\pi C_n(\theta_i)} \left[1 + \cos\theta_i \cos\theta_r - \sin\theta_i \sin\theta_r \cos(\psi_i - \psi_r)\right]^n, \tag{7.21a}$$

$$C_n(\theta_i) = \frac{1}{\pi} \int_0^{2\pi} \int_0^{\pi/2} (1 + \cos\theta_i \cos\theta + \sin\theta_i \sin\theta \cos\psi)^n \cos\theta \sin\theta \, d\theta \, d\psi. \tag{7.21b}$$

The bidirectional reflection function within the plane of incidence ($\psi_r = \psi_i$ or $\psi_i + \pi$) is shown in Fig. 7-4*b* for two different incidence directions and three different values of n. Obviously, for $n = 0$ the surface reflects diffusely (but the *amount* of reflection, as well as absorption and emission, depends on direction through Fresnel's equation). As n grows, the surface becomes more specular, and purely specular reflection would be reached with $n \to \infty$. For this configuration and surface material we should like to determine the heat lost from the plates using the net radiation method.

As indicated in Fig. 7-4*a* we shall apply the net radiation method, equations (7.18) and (7.20), by breaking up each surface into $M \times N$ subsurfaces (M divisions in the x- and y-directions, N in the z-direction). Considering the intensity at node (i, k) on the bottom surface directed toward node (j_o, k_o) on the vertical wall, we find that equation (7.18) becomes, after division by I_b,

$$\Phi_{i,k\to j_o,k_o} = \frac{I_{i,k\to j_o,k_o}}{I_b} = \epsilon_{i,k\to j_o,k_o} + \sum_{j_i=1}^{M} \sum_{k_i=1}^{N} \pi\rho_{j_i,k_i\to i,k\to j_o,k_o} F_{i,k\to j_i,k_i} \Phi_{j_i,k_i\to i,k}. \tag{7.22}$$

In this relation we have made use of the fact that a node on the bottom surface can only see nodes on the side wall and vice versa. Also, by symmetry we have

$$\Phi_{i,k\to j_o,k_o} = \Phi_{j,k\to i_o,k_o} \quad \text{if} \quad j = i \quad \text{and} \quad i_o = j_o,$$

and

$$\Phi_{i,k\to j_o,k_o} = \Phi_{i,N+1-k\to j_o,N+1-k_o},$$

that is, the intensity must be symmetric to the two planes $x = y$ and $z = L/2$. We, therefore, have a total of $M \times (N/2)$ unknowns (assuming N to be even) and need to apply equation (7.22) for $i = 1, 2, \ldots, M$ and $k = 1, 2, \ldots, N/2$. To calculate the necessary ϵ' and ρ'' values, one must establish a number of polar and azimuthal angles. From Fig. 7-4*a* it follows that

$$(\cos\theta_i)_{i,k\to j_i,k_i} = \frac{y_{j_i}}{\sqrt{x_i^2 + y_{j_i}^2 + (z_k - z_{k_i})^2}},$$

$$(\cos\theta_r)_{i,k\to j_o,k_o} = \frac{y_{j_o}}{\sqrt{x_i^2 + y_{j_o}^2 + (z_k - z_{k_o})^2}}.$$

Using the values for $(\cos\theta_r)_{i,k\to j_o,k_o}$ one can readily calculate the directional emittances $\epsilon_{i,k\to j_o,k_o} = 1 - \rho'(\cos\theta_r)$ from Fresnel's equation as given in Example 7.3. Similarly, $\rho'(\cos\theta_i)$ and $C_n(\cos\theta_i)$ are determined from Fresnel's equation and equation (7.21),[3] respectively; and all values of $\rho_{j_i,k_i\to i,k\to j_o,k_o}$ follow from equation (7.21). All necessary view factors may be calculated from equation (4.41), for

[3]For integer values of n the integration may be carried out analytically, either by hand or on a computer using a symbolic mathematics analyzer (the latter having been used here).

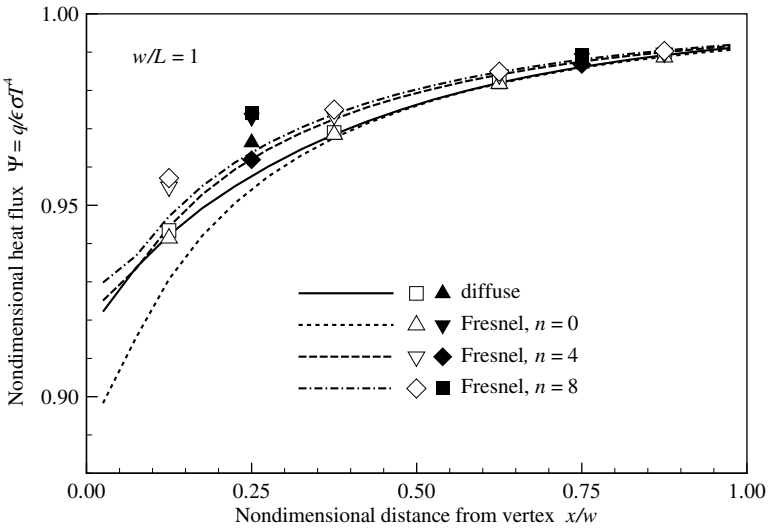

FIGURE 7-5
Nondimensional, local heat fluxes for the corner geometry of Example 7.4, for $w/L = 1$. Solid symbols: Surfaces are broken up into 2×2 subsurfaces; open symbols: 4×4 subsurfaces; lines: 20×20 subsurfaces.

arbitrarily oriented perpendicular plates. For all view factors the opposing surfaces are of identical and constant size with $x_2 - x_1 = y_2 - y_1 = w/M$ and $z_1 = z_3 - z_2 = L/N$. Offsets x_1 and y_1 may vary between 0 and $(M-1)w/M$ and z_2 between 0 and $(N-1)L/N$. Thus, using symmetry and reciprocity, one must evaluate a total of $(M/2) \times M \times N$ view factors. In many of today's workstations and computers all different values of directional emittance, the factor ρ'/C_n in the bidirectional reflection function, and all view factors may be calculated—once and for all—and stored (requiring memory allocation for often millions of numbers). The bidirectional reflection function itself depends on surface locations and on all possible incoming as well as all possible outgoing directions. Even after employing symmetry and reciprocity (for the bidirectional reflection function), this would require storing $[M \times (N/2)] \times [M \times N]^2/2 = (MN)^3/4$ numbers. Unless relatively few subdivisions are used (say $M, N < 10$), it will be impossible to precalculate and store values of the bidirectional reflection function; rather, part of it must be recalculated every time it is required.

The nondimensional intensities are now easily found from equation (7.22) by successive approximation: A first guess for the intensity field is made by setting $\Phi_{i,k \to j_o,k_o} = \epsilon_{i,k \to j_o,k_o}$. Improved values for $\Phi_{i,k \to j_o,k_o}$ are found by evaluating equation (7.22) again and again until the intensities have converged to within specified error bounds. The local net radiative heat flux may then be determined from equation (7.20*b*) as

$$\Psi_{i,k} = \frac{q_{i,k}}{\epsilon E_b} = 1 - \frac{1}{\epsilon} \sum_{j_i=1}^{M} \sum_{k_i=1}^{N} \epsilon_{i,k \to j_i,k_i} F_{i,k \to j_i,k_i} \Phi_{j_i,k_i \to i,k}.$$

Some representative results for the local radiative heat flux near $z = L/2$ (i.e., for $k = N/2$) are shown in Fig. 7-5 for the case of $w = L$ (square plates). Clearly, taking into consideration substantially different reflective properties has rather small effects on the local heat transfer rates. Obviously, as the surface becomes more specular (increasing n) the heat loss rates increase (since less radiation will be reflected back to the emitting surface), but the increases are very minor except for the region close to the vertex (and even there, they are less than 4%).

The directional distribution of the emittance is just as important as that of the bidirectional reflection function: The curve labeled "diffuse" shows the case of diffuse emission and reflection, i.e., $\epsilon'(\hat{\mathbf{s}}) = \alpha'(\hat{\mathbf{s}}) = \epsilon = 0.1$ and $\pi\rho''(\hat{\mathbf{s}}_i, \hat{\mathbf{s}}_r) = \rho' = 1 - \epsilon = 0.9$. In contrast, the curve labeled "Fresnel, $n = 0$" corresponds to the case of $\epsilon'(\hat{\mathbf{s}}) = \alpha'(\hat{\mathbf{s}}) = 1 - \rho'(\hat{\mathbf{s}})$ evaluated from Fresnel's equation and $\pi\rho(\hat{\mathbf{s}}_i, \hat{\mathbf{s}}_r) = \rho'(\hat{\mathbf{s}}_i)$. All lines in Fig. 7-5 have been calculated by breaking up each surface into 20×20 subsurfaces. Also included are the data points for results obtained by breaking up each surface into only 2×2 (solid symbols) and 4×4 surfaces (open symbols). Local heat fluxes are predicted accurately with few subsurfaces, even for

strongly nondiffuse reflection. Total heat loss is predicted even more accurately, with maximum errors of $< 0.6\%$ (2×2 subsurfaces) and $< 0.3\%$ (4×4 subsurfaces), respectively.

The results should be compared with those of Toor [7] for $w/L \to 0$, as shown in Fig. 6-17: The "diffuse" case of Fig. 7-5 virtually coincides with the corresponding case in Fig. 6-17, while the $n = 8$ case falls very close to the specular case with Fresnel-varying reflectance of Toor (solid line in Fig. 6-17).

For the present example at least, taking into account the directional behavior of emittance and reflectance is rarely justifiable in view of the additional complexity and computational effort required. Only if the radiative properties are known with great accuracy, and if heat fluxes need to be determined with similar accuracy, should this type of analysis be attempted. Similar statements may be made for most other configurations. For example, if Example 7.4 is recalculated for directly opposed parallel quadratic plates, the effects of Fresnel's equation and the bidirectional reflection function are even less: Heat fluxes for diffuse reflection—whether Fresnel's equation is used or not—differ by less than 0.6%, while differences due to the value of n in the bidirectional reflection function never exceed 0.2%. Only in configurations with collimated irradiation and/or strong beam-channeling possibilities should one expect substantial impact as a result of the directional variations of surface properties.

7.4 ANALYSIS FOR ARBITRARY SURFACE CHARACTERISTICS

The discussion in the previous two sections has demonstrated that the evaluation of radiative transfer rates in enclosures with nonideal surface properties, while relatively straightforward to formulate, is considerably more complex and time-consuming. If one considers nongray surface properties, the computational effort increases roughly by a factor of M if M spectral bands (band approximation) or M sets of property values (semigray approximation) are employed. In an analysis with directional properties for an enclosure with N subsurfaces, the computational effort is increased roughly by a factor of N (an enormous increase if a substantial number of subdivisions are made). If the radiative properties are both nongray and directionally varying, the problem becomes even more difficult. While it is relatively simple to combine the methods of the previous two sections for the analysis of an enclosure with such surface properties, to the author's knowledge this has not yet been done in any reported work. Few analytical solutions for such problems can be found (for the very simplest of geometries), and even standard numerical techniques may fail for nontrivial geometries; because of the four-dimensional character, huge matrices would have to be inverted. Therefore, such calculations are normally carried out with statistical methods such as the Monte Carlo method (to be discussed in detail in Chapter 8). For example, Toor [7] has studied the radiative interchange between simply arranged flat surfaces having theoretically determined directional surface properties; Modest and Poon [11] and Modest [12] evaluated the heat rejection and solar absorption rates of the U.S. Space Shuttle's heat rejector panels, using nongray and directional properties determined from experimental data. The validity and accuracy of several directional models have been tested and verified experimentally by Toor and Viskanta [13,14]. They studied radiative transfer among three simply arranged parallel rectangles, comparing experimental results with a simple analysis employing (*i*) the semigray model, (*ii*) Fresnel's equation for the evaluation of directional properties, and (*iii*) reflectances consisting of purely diffuse and specular parts. They found good agreement with experiment and concluded that, for the gold surfaces studied, (*i*) directional effects are more pronounced than nongray effects, and (*ii*) in the presence of one or more diffusely reflecting surfaces the effects of specularity of other surfaces become unimportant.

Employing a combination of band approximation and the net radiation method has the disadvantage that (*i*) either large amounts of directional properties and/or view factors must be calculated repeatedly in the iterative solution process (making the method numerically inefficient), or (*ii*) large amounts of precalculated properties and/or view factors must be stored

(requiring enormous amounts of computer storage). In addition, this method tends to have a voracious appetite for computer CPU time. On the other hand, it avoids the statistical scatter that is always present in Monte Carlo solutions. In light of today's rapid development in the computer field, with many small workstations and personal computers boasting internal storage capacities of several gigabytes, as well as enormous number-crunching capabilities, it appears that the methods discussed in this chapter may become attractive alternatives to the Monte Carlo method.

References

1. Branstetter, J. R.: "Radiant heat transfer between nongray parallel plates of tungsten," *NASA TN D-1088*, 1961.
2. Armaly, B. F., and C. L. Tien: "A note on the radiative interchange among nongray surfaces," *ASME Journal of Heat Transfer*, vol. 92, pp. 178–179, 1970.
3. Bobco, R. P., G. E. Allen, and P. W. Othmer: "Local radiation equilibrium temperatures in semigray enclosures," *Journal of Spacecraft and Rockets*, vol. 4, no. 8, pp. 1076–1082, 1967.
4. Plamondon, J. A., and C. S. Landram: "Radiant heat transfer from nongray surfaces with external radiation. Thermophysics and temperature control of spacecraft and entry vehicles," *Progress in Astronautics and Aeronautics*, vol. 18, pp. 173–197, 1966.
5. Shimoji, S.: "Local temperatures in semigray nondiffuse cones and v-grooves," *AIAA Journal*, vol. 15, no. 3, pp. 289–290, 1977.
6. Dunkle, R. V., and J. T. Bevans: "Part 3, a method for solving multinode networks and a comparison of the band energy and gray radiation approximations," *ASME Journal of Heat Transfer*, vol. 82, no. 1, pp. 14–19, 1960.
7. Toor, J. S.: "Radiant heat transfer analysis among surfaces having direction dependent properties by the Monte Carlo method," M.S. thesis, Purdue University, Lafayette, IN, 1967.
8. Hering, R. G., and T. F. Smith: "Surface roughness effects on radiant energy interchange," *ASME Journal of Heat Transfer*, vol. 93, no. 1, pp. 88–96, 1971.
9. Hering, R. G., and T. F. Smith: "Apparent radiation properties of a rough surface," AIAA paper no. 69-622, 1969.
10. Bevans, J. T., and D. K. Edwards: "Radiation exchange in an enclosure with directional wall properties," *ASME Journal of Heat Transfer*, vol. 87, no. 3, pp. 388–396, 1965.
11. Modest, M. F., and S. C. Poon: "Determination of three-dimensional radiative exchange factors for the space shuttle by Monte Carlo," ASME paper no. 77-HT-49, 1977.
12. Modest, M. F.: "Determination of radiative exchange factors for three dimensional geometries with nonideal surface properties," *Numerical Heat Transfer*, vol. 1, pp. 403–416, 1978.
13. Toor, J. S., and R. Viskanta: "A critical examination of the validity of simplified models for radiant heat transfer analysis," *International Journal of Heat and Mass Transfer*, vol. 15, pp. 1553–1567, 1972.
14. Toor, J. S., and R. Viskanta: "Experiment and analysis of directional effects on radiant heat transfer," *ASME Journal of Heat Transfer*, vol. 94, pp. 459–466, November 1972.

Problems

7.1 Two identical circular disks of diameter $D = 1$ m are connected at one point of their periphery by a hinge. The configuration is then opened by an angle ϕ. Disk 1 is a diffuse reflector, but emits and absorbs according to

$$\epsilon'_\lambda = \begin{cases} 0.95 \cos\theta, & \lambda \le 3\,\mu\text{m}, \\ 0.5, & \lambda > 3\,\mu\text{m}. \end{cases}$$

Disk 2 is black. Both disks are insulated. Assuming the opening angle to be $\phi = 60°$, calculate the average equilibrium temperature for each of the two disks, with solar radiation entering the configuration parallel to Disk 2 with a strength of $q_{\text{sun}} = 1000\,\text{W/m}^2$.

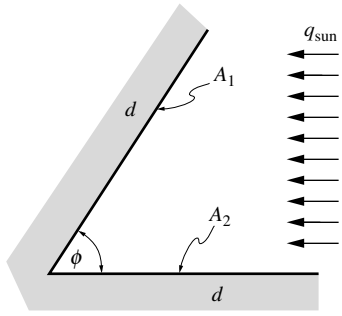

7.2 Reconsider Problem 7.1 for the case that surfaces A_1 and A_2 are long, rectangular plates.

7.3 Repeat Problem 5.17 using the semigray approximation. Disk 1 is covered with a diffuse coating of black chrome (Fig. 3-33).

7.4 Repeat Example 5.8 for an absorber plate made of black chrome (Fig. 3-33) and a glass cover made of soda–lime glass (Fig. 3-28). Use the semigray or the band approximation.

7.5 Repeat Problem 5.36 for the case that the top of the copper shield is coated with white epoxy paint (Fig. 3-33).

7.6 A cubical enclosure has five of its surfaces maintained at 300 K, while the sixth is isothermal at 1200 K. The entire enclosure is coated with a material that emits and reflects diffusely with

$$\epsilon_\lambda = \begin{cases} 0.2, & 0 \le \lambda < 4\,\mu\text{m}, \\ 0.8, & 4\,\mu\text{m} < \lambda < \infty. \end{cases}$$

Determine the net radiative heat fluxes on the surfaces.

7.7 Repeat Problem 6.13 for the case that Surface 1 is coated with the material described in Problem 7.6.

7.8 Repeat Problem 6.26 for the case that the corner is coated with a diffusely emitting, specularly reflecting layer whose spectral behavior may be approximated by

$$\epsilon_\lambda = \begin{cases} 0.8, & 0 \le \lambda < 3\,\mu\text{m}, \\ 0.2, & 3\,\mu\text{m} < \lambda < \infty. \end{cases}$$

The line source consists of a long filament at 2500 K inside a quartz tube, i.e., the source behaves like a gray body for $\lambda < 2.5\,\mu$m but has no emission beyond 2.5 μm.

7.9 Repeat Problem 6.27 for the case that the side wall A_2 is coated with a diffusely emitting, specularly reflecting layer whose spectral behavior may be approximated by

$$\epsilon_\lambda = \begin{cases} 0.1, & 0 \le \lambda < 3\,\mu\text{m}, \\ 0.8, & 3\,\mu\text{m} < \lambda < \infty. \end{cases}$$

7.10 Repeat Problem 5.26 for the case that A_1 is coated with a material that has a spectral, directional emittance of

$$\epsilon'_\lambda = \begin{cases} 0.9\cos\theta, & \lambda < 4\mu\text{m}, \\ 0.3, & \lambda > 4\mu\text{m}. \end{cases} \quad 0 \le \theta < \frac{\pi}{2}.$$

7.11 Consider the configuration shown, consisting of a conical cavity A_1 and an opposing circular disk with a hole at the center, as shown (d = 1 cm). Defocused laser radiation at 10.6 μm enters the configuration through the hole in the disk as shown, the beam having a strength of $q_L = 10^3$ W/cm^2. The down-facing disk A_2 is a gray, diffuse material with $\epsilon_2 = 0.1$, and is perfectly insulated (toward top). Surface A_1 is kept at a constant temperature of 500 K. No other external surfaces or sources affect the heat transfer.

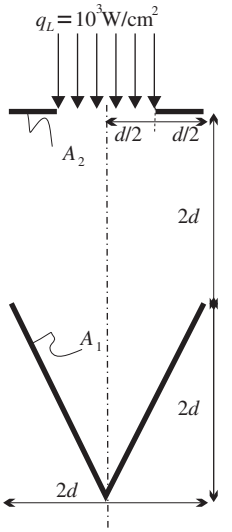

(*a*) Assuming surface A_1 to be gray and diffuse with $\epsilon_1 = 0.3$ determine the amount of heat that needs to be removed from A_1 (Q_1).

(*b*) If A_1 were coated with the material of Problem 3.12, how would you determine Q_1? Set up any necessary equations and indicate how you would solve them (no actual solution necessary). Would you expect Q_1 to increase/decrease/stay the same (and why)?

(*c*) What other simple measures can you suggest to improve the accuracy of the solution (to either *(a)* or *(b)*)?

7.12 During a materials processing experiment on the Space Shuttle (under microgravity conditions) a platinum sphere of 3 mm diameter is levitated in a large, cold black vacuum chamber. A spherical aluminum shield (with a circular cutout) is placed around the sphere as shown, to reduce heat loss from the sphere. Initially, the sphere is at 200 K and is suddenly irradiated with a laser providing an irradiation of 100 W (normal to beam) to raise its temperature rapidly to its melting point (2741 K). Determine the time required to reach the melting point. You may assume the sphere to be essentially isothermal at all times, and the shield to have zero heat capacity. The platinum and aluminum may be taken as diffuse emitters and reflectors with

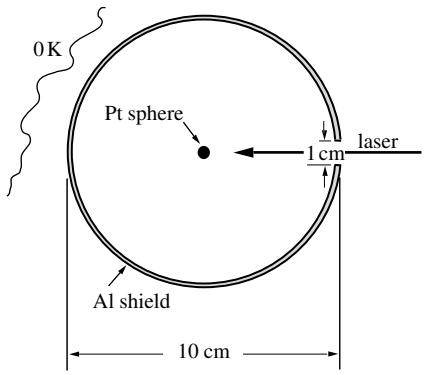

$$\epsilon_{Pt} = \epsilon_{Pt,0}\sqrt{\frac{\lambda_0}{\lambda}} \qquad \epsilon_{Pt,0} = 0.25, \qquad \lambda_0 = 2\,\mu\text{m},$$

$$\epsilon_{Al} = \epsilon_{Al,0}\sqrt{\frac{\lambda_0}{\lambda}} \qquad \epsilon_{Al,0} = 0.1, \qquad \lambda_0 = 2\,\mu\text{m}.$$

(*a*) Use the semigray approximation, using gray values for reemission from sphere and shield.

(*b*) Use the band approximation, splitting the spectrum into three appropriate bands.

7.13 In the solar energy laboratory at UC Merced parabolic concentrators are employed to enhance the absorption of tubular solar collectors as shown in the sketch. Assume that solar energy enters the cavity normal to the opening, with a strength of $q_{\text{sun}} = 1000\,\text{W/m}^2$ (per unit area normal to the rays). The parabolic receiver is coated with a highly reflective gray, diffuse material with $\epsilon_1 = 0.05$, and is kept cold by convection (i.e., emission from it is negligible). Calculate the collected solar energy as a function of tube outer temperature (say, for 300 K, 400 K, 500 K),

(a) assuming the tube to be gray with emittance $\epsilon_2 = 0.90$,

(b) assuming the tube to be covered with black nickel, using the 2-band approach.

It is sufficient to treat tube and concentrator each as single zones.

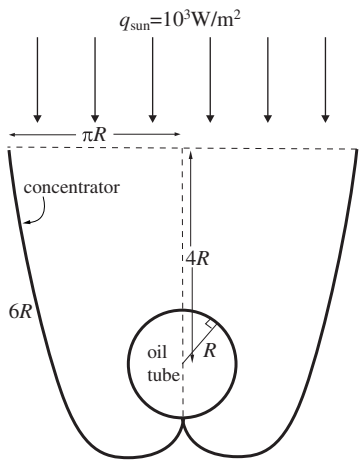

7.14 A small spherical heat source outputting $Q_s = 10$ kW power, spreading equally into all directions, is encased in a reflector as shown, consisting of a hemisphere of radius $R = 40$ cm, plus a ring of radius R and height $h = 30$ cm. The arrangement is used to heat a disk of radius = 25 cm a distance of $L = 30$ cm below the reflector. Reflector A_2 is gray and diffuse with emittance of $\epsilon_2 = 0.1$ and is insulated. Disk A_1 is diffuse and coated with a selective absorber, i.e.,

$$\epsilon_{1\lambda} = \begin{cases} 0.8, & 0 \le \lambda < 3\,\mu\text{m}, \\ 0.2, & 3\,\mu\text{m} < \lambda < \infty. \end{cases}$$

The source is of the tungsten–halogen type, i.e., the spectral variation of its emissive power follows that of a blackbody at 4000 K.

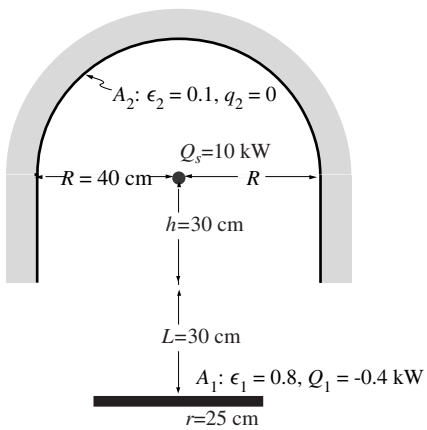

(*a*) Determine (per unit area of receiving surface) the irradiation from heat source to reflector and to disk.

(*b*) Determine all relevant view factors.

(*c*) Outline how you would obtain the temperature of the disk, if 0.4 kW of power is extracted from it. ("Outline" implies setting up all the necessary equations, plus a sentence on how you would solve them.)

7.15 Repeat Problem 7.8 using subroutine `bandapp` of Appendix F (or modifying the sample program `bandmxch`). Break up each surface into N subsurfaces of equal width ($n = 1, 2, 4, 8$).

7.16 Repeat Problem 5.25 for the case that the insulated cylinder is coated with a material that has

$$\epsilon_{2\lambda} = \begin{cases} 0.2, & 0 \le \lambda < 4\,\mu\text{m}, \\ 0.8, & 4\,\mu\text{m} < \lambda < \infty \end{cases}$$

(the flat surface remains gray with $\epsilon_3 = 0.5$). Note that the wire heater is gray and diffuse and at a temperature of $T_1 = 3000$ K.

(*a*) Find the solution using the semigray method; also set up the same problem and find the solution by using program `semigrayxchdf`.

(*b*) Set up the solution using the band approximation, i.e., to the point of having a set of simultaneous equations and an outline of how to solve them. Also find the solution using program `bandmxchdf`.

7.17 Repeat Problem 5.2 assuming that the furnace walls are made of alumina ceramic (aluminum oxide, Fig. 1-14). Use subroutine `bandapp` of Appendix F (or modifying the sample program `bandmxch`). Break up the spectrum into several parts, and compare your results for $N = 1, 2, 3$, and 5.

7.18 Repeat Problem 5.19 assuming that the furnace walls are made of alumina ceramic (aluminum oxide, Fig. 1-14). Use subroutine `semigray` of Appendix F (or modifying the sample program `semigrxch`). Break up the groove surface into N subsurfaces of equal size ($N = 2$ and 4), but only consider incidence angles of $\theta = 0°$ and 60°.

7.19 Repeat Problem 6.26 for the case that the corner is cold (i.e., has negligible emission), and that the surface is gray and specularly reflecting with $\epsilon = \rho^s = 0.5$, but has a directional emittance/absorptance of

$$\epsilon'(\theta) = \epsilon_n \cos\theta.$$

Determine local and total absorbed radiative heat fluxes.

7.20 Consider two infinitely long, parallel plates of width $w = 1$ m, spaced a distance $h = 0.5$ m apart (see Configuration 32 in Appendix D). Both plates are isothermal at 1000 K and are coated with a gray material with a directional emittance of

$$\epsilon'(\theta_i) = \alpha'(\theta_i) = 1 - \rho'(\theta_i) = \epsilon_n \cos\theta_i$$

and a hemispherical emittance of $\epsilon = 0.5$. Reflection is neither diffuse nor specular, but the bidirectional reflection function of the material is

$$\rho''(\theta_i, \theta_r) = \frac{3}{2\pi}\rho'(\theta_i)\,\cos\theta_r.$$

Write a small computer program to determine the total heat lost (per unit length) from each plate. Compare with the case for a diffusely emitting/reflecting surface.